**Article:**
Karali, A., Dall'Ara, E., Zekonyte, J. et al. (2023) Effect of radiation-induced damage of trabecular bone tissue evaluated using indentation and digital volume correlation. Journal of the Mechanical Behavior of Biomedical Materials, 138. 105636. ISSN: 1751-6161

https://doi.org/10.1016/j.jmbbm.2022.105636

journal of the mechanical behavior of biomedical materials 138 (2023) 105636

Contents lists available at ScienceDirect

Journal of the Mechanical Behavior of Biomedical Materials

journal homepage: www.elsevier.com/locate/jmbbm

# Effect of radiation-induced damage of trabecular bone tissue evaluated using indentation and digital volume correlation

Aikaterina Karali [a,*], Enrico Dall'Ara [b], Jurgita Zekonyte [a], Alexander P. Kao [a], Gordon Blunn [c], Gianluca Tozzi [a]

[a] School of Mechanical and Design Engineering, University of Portsmouth, Portsmouth, UK
[b] Departement of Oncology and Metabolism and Insigneo Institute for in Silico Medicine, University of Sheffield, Sheffield, UK
[c] School of Pharmacy and Biomedical Sciences, University of Portsmouth, UK

ARTICLE INFO

*Keywords:*
Indentation
Digital volume correlation (DVC)
Tissue irradiation
X-ray computed tomography (XCT)
Trabecular bone

ABSTRACT

Exposure to X-ray radiation for an extended amount of time can cause damage to the bone tissue and therefore affect its mechanical properties. Specifically, high-resolution X-ray Computed Tomography (XCT), in both synchrotron and lab-based systems, has been employed extensively for evaluating bone micro-to-nano architecture. However, to date, it is still unclear how long exposures to X-ray radiation affect the mechanical properties of trabecular bone, particularly in relation to lab-XCT systems. Indentation has been widely used to identify local mechanical properties such as hardness and elastic modulus of bone and other biological tissues. The purpose of this study is therefore, to use indentation and XCT-based investigative tools such as digital volume correlation (DVC) to assess the microdamage induced by long exposure of trabecular bone tissue to X-ray radiation and how this affects its local mechanical properties. Trabecular bone specimens were indented before and after X-ray exposures of 33 and 66 h, where variation of elastic modulus was evaluated at every stage. The resulting elastic modulus was decreased, and micro-cracks appeared in the specimens after the first long X-ray exposure and crack formation increased after the second exposure. High strain concentration around the damaged tissue exceeding 1% was also observed from DVC analysis. The outcomes of this study show the importance of designing appropriate XCT-based experiments in lab systems to avoid degradation of the bone tissue mechanical properties due to radiation and these results will help to inform future studies that require long X-ray exposure for *in situ* experiments or generation of reliable subject-specific computational models.

## 1. Introduction

Bone is an anisotropic, heterogeneous material, with hierarchical structure (Franzoso and Zysset, 2008; Hengsberger et al., 2003; Oftadeh et al., 2015; Swadener et al., 2001; Wolfram et al., 2010b; Zysset, 2003). In order to evaluate the mechanical behaviour of bone, the properties of its hierarchical structures need to be assessed at different length scales (Buckwalter et al., 1995; Jae-young et al., 1998). The microstructural properties of bone determine its macrostructural behaviour (Oftadeh et al., 2015; Wolfram et al., 2010a), therefore it is important to study its mechanical properties at the micro level.

Tissue level mechanical properties are not affected by the shape and size of the bone. They depend on the mineralisation of the tissue, anisotropic nature of the collagen network and nano-level pores (i.e. lacuna/canalicular network) (Hunt and Donnelly, 2016; Rodriguez-Florez et al., 2013). Indentation testing is an effective way of evaluating bone tissue properties (i.e. elastic modulus and hardness). It has been used extensively in the last few decades to characterise trabecular bone in axial, longitudinal and transverse directions, although it has been noticed that measurements may differ due to the variability of the local pores and heterogeneity of mineralisation (Hengsberger et al., 2003; Hoffler et al., 2000; Zysset, 2009). Moreover, it has been combined with a variety of techniques to better inform computational models (Lucchini et al., 2011; Wolfram et al., 2010b; Zhang et al., 2010) and enhance the understanding of the relation between microscopic and macroscopic bone properties (Mirzaali et al., 2016).

More specifically, X-ray computed tomography (XCT) and indentation have been integrated at different scales (nano and micro) to characterise the bone morphology and mechanical properties. In 2003,

* Corresponding author.
*E-mail address:* katerina.karali@port.ac.uk (A. Karali).

https://doi.org/10.1016/j.jmbbm.2022.105636
Received 27 January 2022; Received in revised form 9 December 2022; Accepted 19 December 2022
Available online 20 December 2022

Hengsberger et al., estimated the local anisotropic elastic constants of cortical bone using Synchrotron X-ray computed tomography (SR-XCT) to calculate the porosity prior to obtaining the apparent longitudinal modulus via nanoindentation (Hengsberger et al., 2003). Different regions of the same specimens were used for nanoindentation and imaging, to ensure that mechanical properties of the tissue were not compromised by the radiation. Furthermore Harrison et al., used finite element (FE) modelling of trabecular bone with heterogenity of the tissue modulus informed from nanoindentation measurements and local heterogenity in the grey levels obatained from lab-based XCT scans (Harrison et al., 2008). Similar to Hengsberger et al., they used different parts of the same specimen for the imaging and indentation. More recently, Lowe et al., performed an *in situ* high-resolution XCT indentation in dried mouse femoral head, using a lab-XCT system, to visualise and track plastic deformation and crack propagation; an experiment that lasted 52 h (Lowe et al., 2018). Conventional lab-based XCTs use polychromatic x-ray cone beam, whereas Synchrotron CTs use monochromatic parallel beam. The radiation of Synchrotron systems has a higher flux compared to conventional lab based XCTs, that have limited photon emissions (Chappard et al., 2006). However, to optimise the quality of a lab-based XCT high-resolution scan a higher signal-to-noise ratio (SNR) is needed, and thus the acquisition time is increased. This leads to increased X-ray irradiation in the tissue that negatively affects its mechanical properties (Akkus et al., 2005).

High-resolution XCT has been also combined with *in situ* mechanical testing (4D evaluations) and employed to study bone micromechanical properties and behaviour (Tozzi et al., 2014, 2016). In these studies, the deformation induced by compression was analysed using digital volume correlation (DVC). DVC is a three-dimensional technique where the full-field strain distribution is derived on the measured displacement field, which is computed based on the differential variation of grey level intensity for XCT images of the material undergoing *in situ* step-wise loading (Bay et al., 1999; Bonithon et al., 2021; Karali et al., 2020; Tozzi et al., 2017). Peña-Fernández et al. assessed the influence of the radiation dose on the trabecular bone tissue by varying the exposure times within a SR-XCT system (Peña-Fernández et al., 2018a). It was noticed that highly irradiated specimens developed more microcracks within the tissue and the strain distribution in these regions reached 1%. Another study (Peña-Fernández et al., 2018b) retained the bone tissue integrity by performing *in situ* SR-XCT, while controlling the temperature at 23 °C and 0 °C. It was observed that the decrease in the temperature promoted tissue preservation, as there were no visilbe microcracks and the peak values of the first and third principal strains were below ±0.1%. This was, probably, due to the reduction of the cross-linking reactions, of highly reactive oxygen free radicals produced by high-energy X-ray radiation, within the collagen fibres.

However, to the best of the authors knowledge an assessment of the effect of XCT radiation in a lab-system and how this is linked to potential variation of local mechanical properties, has not been investigated. Therefore, the aim of this study is to evaluate trabecular bone tissue damage induced by X-ray irradiation by combining indentation and high-resolution XCT, using DVC to evaluate the strain distribution corresponding to microdamage (i.e. formation of microcracks) induced in the trabeculae by prolonged X-ray exposure.

## 2. Materials and methods

A schematic diagram with detailed description of the experimental protocol is given in Fig. 1.

### 2.1. Materials

Using a diamond band saw (Exact GmbH, Germany) 5 mm high slices of bone were cut from three porcine lumbar vertebrae under constant irrigation. Seven bone plugs, of 3 mm diameter, were cored from different locations within the slices along the axial direction (Fig. 1A). The specimens (S1–S7) were dried at room temperature overnight, then, they were embedded in epoxy resin under vacuum (Epofix, Struers, Denmark), polished with progressive grades of sandpapers (P500, P1000, P2400 and P4000, Struers, Denmark) and Alumina paste using distilled water as a lubricant (Dall'Ara et al., 2013).

### 2.2. Experimental protocol

A first set of indentations was performed prior to the XCT imaging, to evaluate the effect the X-ray radiation had on bone tissue. An average number of 30 indents was performed in specific locations (i.e. avoiding lacunae and away from the edges (Wolfram et al., 2010a)), identified using the integrated optical microscope of the nanoindenter. The diameter of the specimens was reduced by means of milling to 1 mm to facilitate the high-resolution XCT imaging. The resulting specimens included a few trabeculae and a reduced number of indents was performed, whilist keeping a minimum distance of 20 μm from previous indents (Dall'Ara et al., 2013; Wolfram et al., 2010a). This indentation set was executed to access potential damage of the tissue due to the milling. Afterwards, the specimens were exposed to radiation for several hours ($h_x$, where h is the time and $x$ represents the number of hours), depending on the acquisition time of the tomograms. The first overview scan, to visualise the trabecular microstructure at and below the indentation site, was completed after the 2nd indentation set ($h_3$), directly followed by a higher-resolution zoom-in scan on a single indent location ($h_{33}$). Similarly, to examine the effect of radiation exposure in the trabeculae, another overview ($h_{36}$) and high-resolution zoom-in scan ($h_{66}$) were executed after the 3$^{rd}$ indentation set. The final overview scan was acquired to identify the effect the radiation has on the trabeculae ($h_{69}$) (Fig. 1C). Indentations of different sets were placed at a close proximity (i.e. on the same trabecula and within the range of 30–180 μm) to allow comparison of the values before and after irradiation of the tissue.

The first specimen (S1) was tested as control for the mechanics. Overview scans were obtained and the specimen was indented after each overview tomogram to assess the effect of $h_3$, $h_6$ and $h_9$ irradiation on the mechanical properties of the tissue. Initially, specimen diameter including the excess epoxy surrounding the bone was 10 mm. The epoxy was then removed by means of milling after the first indentation set and the diameter remained 3 mm throughout the rest of the process (Fig. 3), which allowed a larger number of indentations in each set.

The temperature was monitored, to ensure no cracks were forming due to expansion or contraction. A thermocouple was attached onto a specimen aligned with the X-ray beam and an overview and high-resolution scan were acquired. It should be noted that the tomograms from these scans were not used for the analysis, only the temperature readings were of interest.

Furthermore, indentations were randomly placed on the epoxy surrounding the trabeculae on three of the specimens throughout the protocol to calculate the potential effect of radiation on the epoxy. The experimental protocol was completed within 6 months of the specimen preparation.

### 2.3. Ex situ indentation

Indentations were performed in dry condition on the embedded and polished specimens using a NanoTest Platform 3 (Micro Materials, UK) nanoindenter, using a Berkovich tip. To maintain the consistency between the NanoTest Platmorm and the subsequent XCT scanning, a mounting set up was designed where the specimen was fixed onto a steel pin (Fig. 1B). Depth control indentation mode was chosen, with the maximum depth set at 2.5 μm (Wolfram et al., 2010c). To minimise the creep effect, a 30s holding time was introduced between the loading and unloading stage. Both the loading and unloading rate was set at 0.8 mN/s (Wolfram et al., 2010c). The indentations were carefully placed to avoid any defects and inhomogeneities in the tissue (Rho et al., 1999).

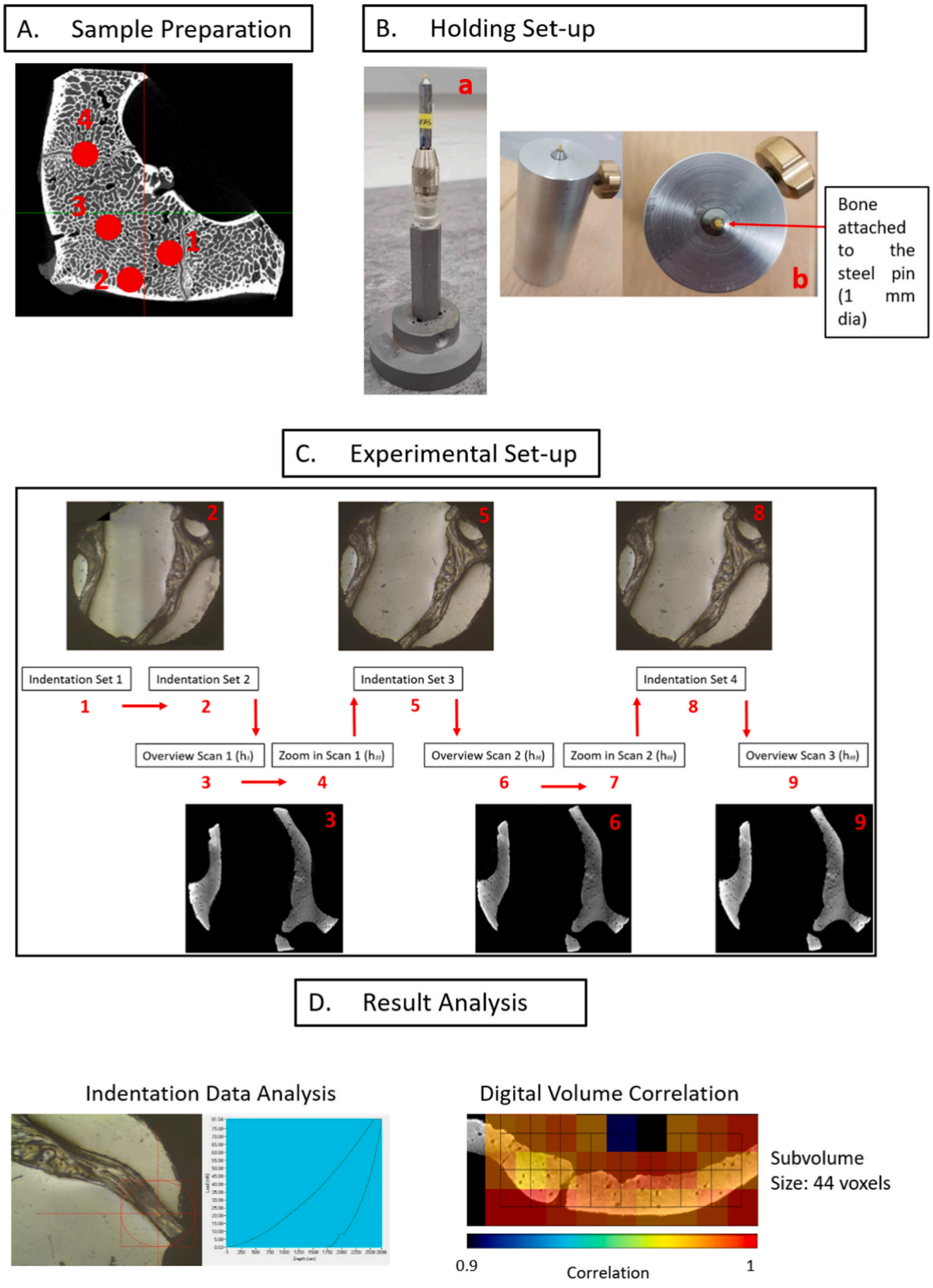


**Fig. 1.** A. Bone plugs (D = 3 mm) extracted from the anterior part of the vertebral body in positions indicated by the red dots (n = 1 in position 1, n = 2 in position 2, n = 1 in position 3 and n = 1 in position 4). B. Holding setup for the (a) XCT system and (b) microindenter. **C.** Experimental testing outline guided by red arrows for step sequence. The first indentation set was performed on D = 3 mm samples, then the sample diameter was reduced to 1 mm for the remaining tests. Indentation location (1,2,5,8) and XCT details of trabeculae after each indentation set (3,6,9) are also shown. **D.** (right) The elastic modulus and hardness were extracted from indentation data of the trabecular bone; (left) DVC analysis performed on the XCT images.

The elastic modulus (E) and hardness (H) were calculated using the Oliver and Pharr method (Oliver and Pharr, 2004), considering local isotropy and Poisson's ratio equal to 0.3 (Harrison et al., 2008).

### 2.4. High resolution XCT imaging

At defined indentation steps, as reported in Fig. 1C, the specimens were XCT imaged (Versa 510, Zeiss, USA). As shown in Table 1 the overview scan was performed at 1.86 μm of voxel size, which allows the whole geometry of the specimen to be in the field of view (FOV) (Fig. 2), whereas in the higher-resolution zoom in scan the voxel size was reduced to 0.13 μm. The images were reconstructed and each 3D dataset consisted of 991 images (984 × 1009 pixels, 16-bit grey levels). After conversion of the images to 8-bit, they were rigidly registered with a correlative metric (Fiji 1.53c, USA) and cropped to parallelepipeds in the centre of the specimens. A mean filter was applied to reduce the noise and a zero-intensity value was introduced to the non-bone voxels by applying a mask to each dataset (Palanca et al., 2015; Peña-Fernández et al., 2018b). The mask was created by executing an arithmetic and logical operation between the original dataset and their respective binary image (Karali et al., 2020, 2021; Peña-Fernández et al., 2018b).

### 2.5. Digital volume correlation

DVC on the XCT images (sequential overview scans) was computed using sum of differential correlation with a multi-pass processing, 74 to 44 voxels of subvolume size (DaVis 10.0.5, LaVison, Göttingen, Germany) (Bonithon et al., 2021; Karali et al., 2020; Tozzi et al., 2016). The error uncertainty was calculated using two repeated overview scans of an 1 mm diameter specimen (S2) (303 ± 140 με) (Palanca et al., 2016; Tozzi et al., 2017). These tomograms were used to compute the error uncertainty as well as the strain induced by radiation at $h_9$. The correlation coefficient was filtered at 0.9 and a geometric mask was used to reduce the error uncertainty. The 3rd principal strain ($\varepsilon_{p3}$), identifying compressive strains, and the maximum shear strain ($\gamma_{max}$) were computed to evaluate the radiation damage.

## 3. Results

Both the elastic modulus and hardness of the S1, which had not been exposed to the high-resolution zoom in scan irradiation, showed a similar median throughout the four different indentation sets. There was a trend of decreased E after $h_6$ (Fig. 3B). The elastic modulus in the first step was 15.8 ± 1.8 GPa (Median ± Standard Deviation) and after the 6 h of radiation exposure it was 14.19 ± 2.1 GPa. Whereas, the H remained approximately the same; with a median of 0.58 ± 0.057 GPa and 0.58 ± 0.049 GPa in the first and last step respectively (Fig SM1). Furthermore, when observing the individual indentations, there was no large variation in the elastic modulus and hardness locally (i.e. 3 b and 3c to 1 b) (Fig. 3. A). The three overview scans showed no visible cracks.

The specimens which were exposed up to 69 h of radiation showed different trends in their E in relation to exposure time. As shown in Fig. 4B, the elastic modulus of S3 at the initial state of the specimen (33 indents) (D = 3 mm) was 10.74 ± 1.85 GPa, which after $h_{66}$ was increased, reaching a maximum value, among the indentations, of 16.33 GPa S4 (Fig. 5A) showed a decrease in the moduli. More specifically, the E of the first indentation set (N = 30 at $h_0$) was 14.24 ± 2.69 GPa. The maximum and minimum values of E in the final set of indentations (N = 6 at $h_{66}$) were 7.99 GPa and 4.88 GPa, respectively. Similarly, the E for S5 (Fig. 5B) for the initial set of indentations (N = 26 at $h_0$) was 14.26 ± 2.48 GPa. For the final set of indentations, the maximum value of E decreased to 7.39 GPa (N = 3 at $h_{66}$). The bone structure in S6 (Fig. 5C) allowed a larger number of indents in the first and last sets, 42 and 5 indentations, respectively. The E for the initial set of indentations was 14.89 ± 2.26 GPa and in the final set of indentations E reached a maximum value of 24.48 GPa. In S7 (Fig. 5D) the E for the first set of indentations (N = 36 at $h_0$) was 14.79 ± 2.93 GPa and the maximum E in the final set of indentations (N = 4 at $h_{66}$) was 22.34 GPa.

**Table 1**
XCT scanning specifications used in this study for overview and higher-resolution imaging.

| | Overview Scan | Higher-resolution Zoom in Scan |
|---|---|---|
| **Objective** | 4X | 40X |
| **Binning** | 2 | 1 |
| **kVolt/Watt** | 60/5 | 80/7 |
| **Filter** | Air | Air |
| **Projections** | 2001 | 2101 |
| **Exposure time (s)** | 1.5 | 46 |
| **Pixel size (μm)** | 1.86 | 0.13 |

The hardness readings varied among the specimens (Fig SM2). The median hardness of S3 in the initial state of the specimen was 0.90 ± 0.06 GPa, which reached a maximum indentation value after $h_{66}$ of 0.64 GPa. The H in S4 showed a similar relationship to increasing radiation to that seen for the values of elasticity at the first indentation set (N = 30 at $h_0$) H was 1.16 ± 0.10 GPa. Whilst, the maximum and minimum values of H in the last set of indentations (N = 6 at $h_{66}$) were 0.63 GPa and 0.25 GPa, respectively. Likewise, the median hardness in S5 0.94 ± 0.10 GPa at $h_0$ (N = 26) and reached a maximum value of 0.47 GPa at $h_{66}$ (N = 3). The hardness at S6 and S7 reached 0.55 ± 0.08 and 0.92 ± 0.96 GPa at $h_0$ with maximum values of 1.00 and 0.96 GPa respectively at the last indentation set ($h_{66}$).

DVC was used to assess the strain induced on the tissue at increasing levels of X-ray exposure. Analysis on S4 for the 3rd principal strain ($\varepsilon_{p3}$) showed higher values around the areas where cracks were formed at $h_{36}$, which were even further damaged at $h_{69}$ (Fig. 6A). Similar pattern appeared for the max shear strain ($\gamma_{max}$). The strain initially reached 1% around the cracks, approaching 2% at $h_{69}$ in the same area without further crack propagation (Fig. 6B).

S5 was the specimen with the largest crack formation; at $h_{69}$ the 3rd principal strain ($\varepsilon_{p3}$) in the trabeculae exceeded absolute principal strains of 1% (Fig. 7A). An increase of strain between the $h_{36}$ and $h_{69}$ also occurred in the max shear strain ($\gamma_{max}$), which exceeded 1% at the last stage (Fig. 7B).

Crack formation is also visible at the higher-resolution XCT of the trabecular bone. Particularly, in S3 cracks are forming at $h_{66}$ (Fig. 8B), starting from the edges of the tissue propagating to the centre. In S4 however, there is crack formation from the first zoom in scan ($h_{33}$, Fig. 8C). As reported in Fig. 8C one of the cracks is starting gradually from the edge of the trabecula and at $h_{66}$ it reaches the nearest lacuna propagating further (Fig. 8D). Whereas the second crack is starting from a lacuna in the middle of the structure at $h_{33}$ propagating towards the boarders at $h_{66}$.

In addition to the XCT image acquisition, the temperature was monitored during imaging and in the overview scan ($h_3$) the temperature increased by 2 °C and remained at the same level through the zoom in scan ($h_{33}$).

## 4. Discussion

The aim of the present study was to investigate the effect of high-resolution XCT radiation on trabecular bone tissue at the micro level. High-resolution XCT has been extensively used to assess the microstructure of trabecular bone (Gillard et al., 2014; Judex et al., 2003; Levrero-Florencio et al., 2016). To investigate features in the micro/nano-scale, such as the residual deformation of the bone caused by the indentation and additionally extract important and more localised mechanical properties of bone tissue (i.e. via DVC), high-resolution and long exposure scans are required (Lowe et al., 2018; Peña Fernández et al., 2019). Long exposure to radiation is known to affect the mechanical properties of cortical bone and cartilage (Akkus et al., 2005; Barth et al., 2010; Tozzi et al., 2020), however it has not yet been

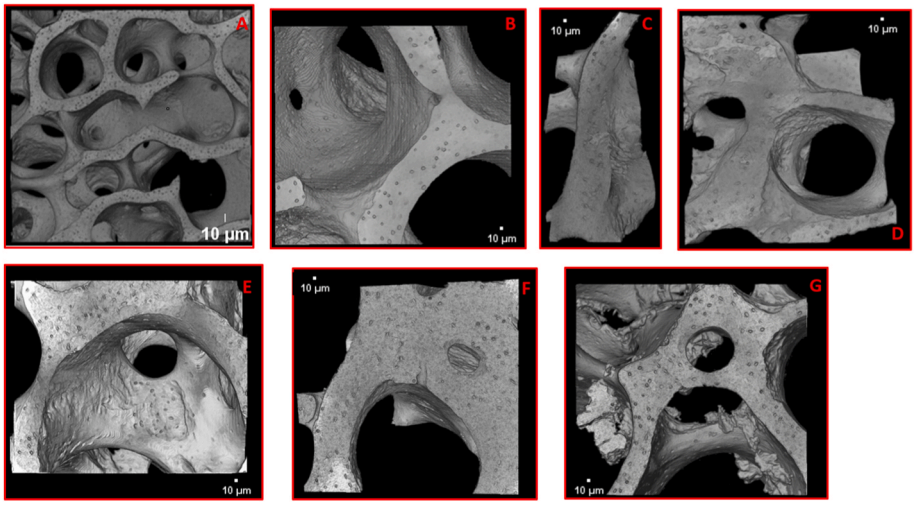


**Fig. 2.** XCT images showing the indentation sites, (A): D = 3 mm mechanics control sample (S1), (B): D = 1 mm imaging control sample (S2), (C–E) D = 1 mm samples following the main experimental protocol S3-7. All samples showed no visible damage after the first image acquisition ($h_3$).

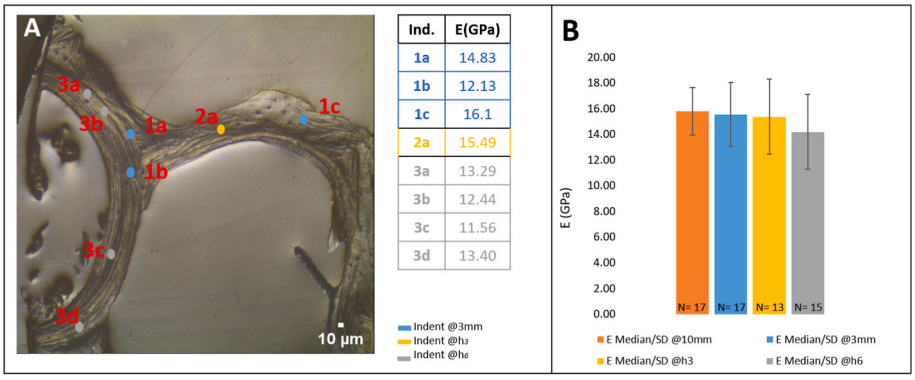


**Fig. 3.** Mechanics control specimen indentation (S1): (A) Trabeculae under optical microscope, with different sets of indents identified and coloured respectively (blue: indents at $h_0$ when specimen diameter was D = 3 mm, yellow: indents after $h_3$ and D = 3 mm grey: indents after $h_6$ and D = 3 mm). (B) Median/SD of elastic modulus of indentation sets (orange: median when specimen diameter was D = 10 mm, blue: median when specimen diameter was D = 3 mm, yellow: median after $h_3$ and D = 3 mm, grey: median after $h_6$ and D = 3 mm).

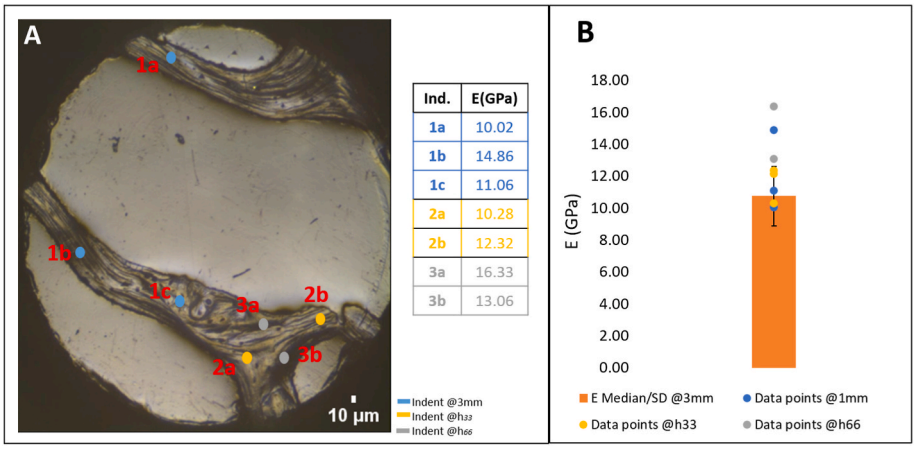


**Fig. 4.** S3: (A) Trabeculae under optical microscope, with different sets of indents identified and coloured respectively (blue: indents at $h_0$ when specimen diameter was D = 1 mm, yellow: indents after $h_{33}$ and D = 1 mm, grey: indents after $h_{66}$ and D = 1 mm). (B) Median/SD of elastic modulus of trabeculae at $h_0$ (orange) and elastic modulus of each indent for the following indentation sets at increasing exposure to X-ray radiation (blue: $h_0$ and D = 1 mm, yellow: $h_{33}$ and D = 1 mm, grey: $h_{66}$ and D = 1 mm).

estimated in trabecular bone.

In this study, indentation was performed to assess the bone tissue mechanical properties before and after exposure in the X-CT. High-resolution XCT imaging was employed to visualise the region of indentation and the internal volume underneath the individual indents for subsequent DVC analysis and to visualise for the formation of cracks after radiation exposure.

The average elastic modulus obtained from all the specimens at $h_0$ was 14.5 ± 3.11 GPa, which is in line with values reported in literature for dehydrated human vertebral trabecular bone, 15.4 ± 1 GPa (Wolfram et al., 2010b) and 13.4 ± 2 GPa (Roy et al., 1999). The difference in the two reported values can be attributed to the nature of the bone; porcine and human, as well as the fact that in the first study both thoracic and lumbar vertebrae were investigated.

The first and second indentation set together with the first overview scans (h3) (Fig. 2) showed that machining did not affect the tissue's

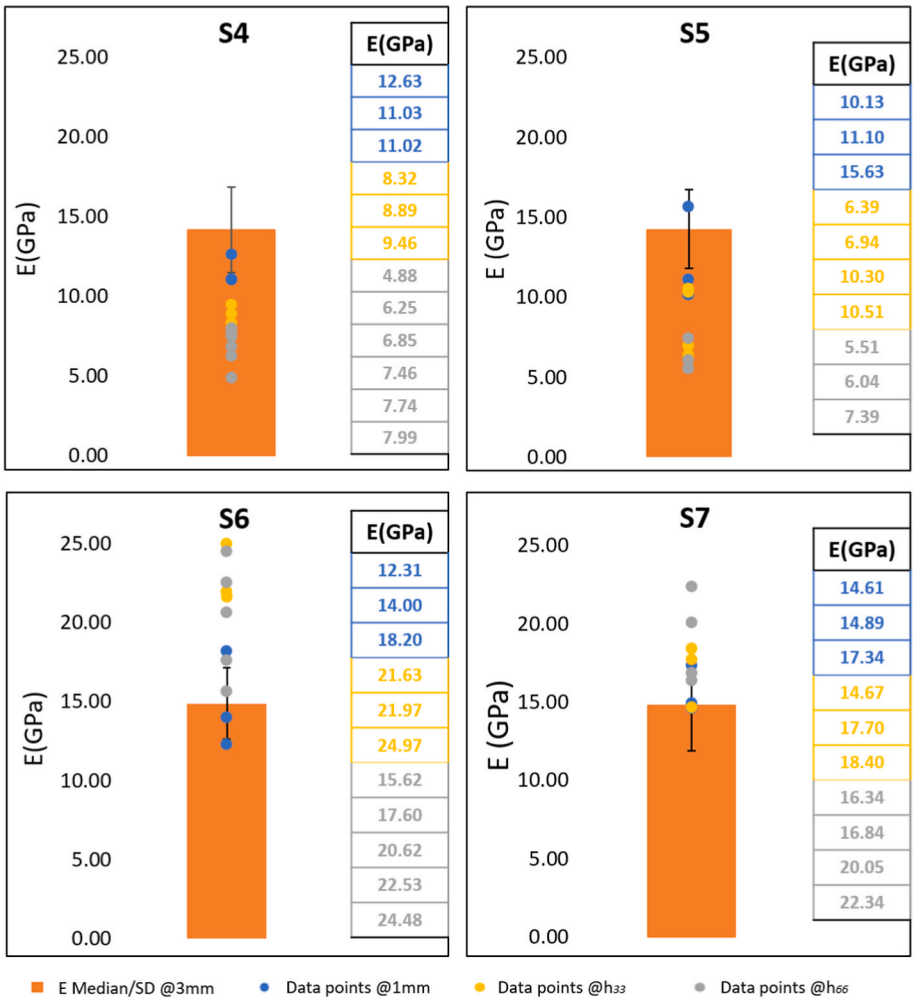


**Fig. 5.** Median/SD elastic modulus at zero exposure to radiation (orange) and elastic modulus of each indent of the following indentation sets at increasing exposure to X-ray radiation stating their values for the remaining samples S4–S7.

mechanical properties and structural integrity. However, change in the mechanical properties, of approximately 13% was observed after the first long exposure scan ($h_{33}$) (Fig. 5). Additionally, after 69 h of scanning, the effect of the radiation was higher. In S3, S6 and S7 the elastic modulus values increased, indicating that the tissue became stiffer (Figs. 4 and 5).

This is even clearer, when comparing individual values of neighbouring indents at $h_0$ and $h_{66}$ as shown in Fig. 4. Specifically, in S3, the indents labelled 1c and 3a in Fig. 4A (at $h_0$ and $h_{66}$ respectively), which are 140 μm away from each other; have a 5.24 GPa difference in the individual calculated E. Local mineralisation and/or local anisotropy of the tissue could be a factor for this difference in the E, however, after radiation exposure there were visible cracks in the region. In S6 at $h_0$ and specimen diameter 3 mm, there were two indents with an elastic modulus of 19.11 and 18.87 GPa spaced 80 μm apart. In the middle of these two at a 30 μm distance two subsequent indents were placed at $h_{33}$ with elastic moduli of 21.63 and 21.97 respectively (Fig. 5C). This shows an increasing trend of approximately 2 GPa even after the first high-resolution zoom in scan.

This trend, however, does not seem to correspond to all the specimens, since S4 and S5 displayed a decrease in the elastic modulus (≈4 GPa) (Fig. 5 A, B). In fact in S5, the indent with modulus 10.13 GPa ($h_0$) (Fig. 5B) has a 30 μm distance from indent with modulus 7.39 GPa ($h_{66}$) in the middle of the same trabecula. Dall'Ara et al. (2012) reported how severe damage, due to compressive deformation (ranging from 12 to 53%), in the trabeculae reduced the indentation moduli and therefore elastic modulus by 55% (Dall'Ara et al., 2012). To such extent, the high-resolution zoom-in tomograms of the tissue showed details in the structure of the trabeculae with clear microdamage that was not visible in the overview tomograms due to the larger voxel size. Microcrack formation might be directly related to the changes in the elastic modulus shown by measurements from the nanoindentation. In S3 the cracks start forming at $h_{66}$ where the modulus is increased, making the tissue stiffer. Whereas in S4, where the modulus shows a continues decrease, the cracks form at $h_{33}$ and propagate further at $h_{66}$, leading to tissue failure as previously observed (Dall'Ara et al., 2012).

The trend of the hardness showed a systematic reduction due to the radiation (Fig.SM1, SM2). This can be attributed to the hardness being primarily affected by the collagen content in the bone (Boivin et al., 2008; Ibrahim et al., 2020; Viguet-Carrin et al., 2006; Wang et al., 2001) whereas the elastic modulus mainly correlates to the mineral content (Huja et al., 2006; Martínez-Reina et al., 2011). Irradiation exposure causes degradation of the collagen due to radiolysis of the water molecules in the bone (Barth et al., 2011; Nguyen et al., 2007). The water that resides in the collagen matrix stabilises the collagen structure, binding molecules through hydrogen bonds; therefore playing a significant role to bone hardness (Dall'Ara et al., 2007; Samuel et al., 2014). In that sense, the decrease in the hardness trend can be potentially attributed to the distortion of collagen matrix due to the irradiation of the bone tissue. However, the impact of the mineral and collagen content has not yet been assessed separately and further investigation is needed.

From the overview scans it was observed that crack formation

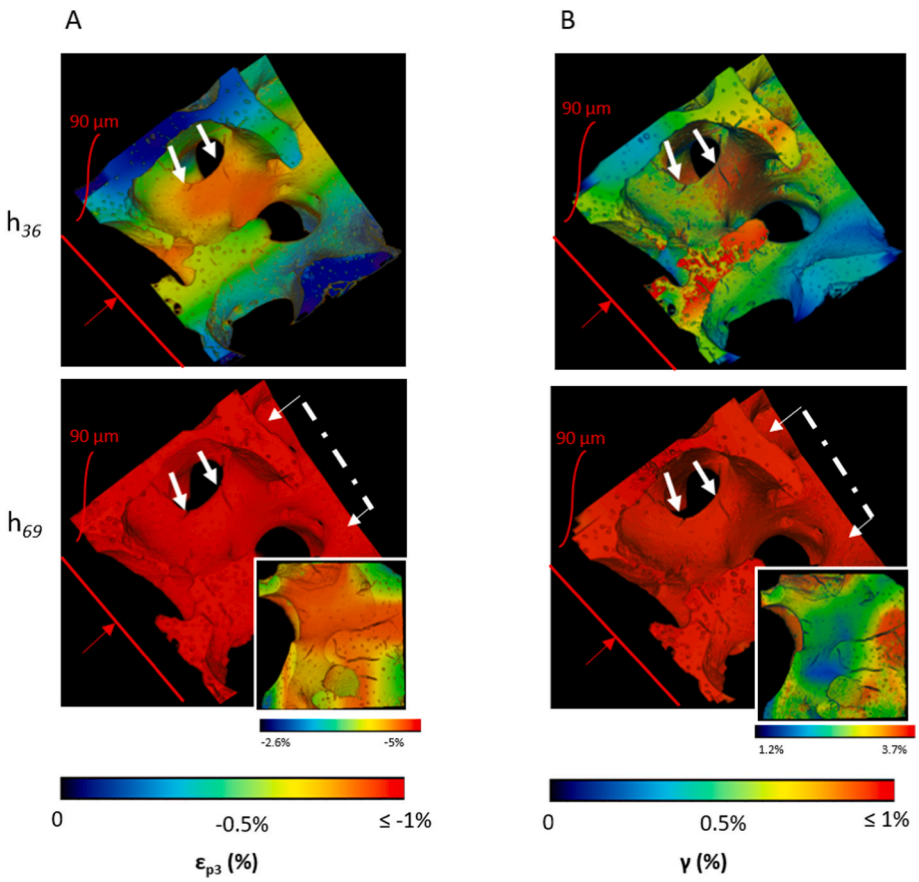


**Fig. 6.** DVC analysis of S4, where red line identifies the indentation plane and red arrow direction (90 µm apart from the represented volume). A) 3rd principal strain ($\varepsilon_{p3}$) at $h_{36}$ and $h_{69}$ reaching ~ -0.8% at areas of crack formation (white arrows) and exceeding −1% throughout the volume, respectively. B) maximum shear strain ($\gamma_{max}$) at the same time points, reaching strains over 3% around the cracks (white arrows) after $h_{69}$. Maximum strain distribution around cracks at $h_{69}$ for cross section are reported at the bottom right corner.

occurred in all the specimens after the first long exposure followed by crack propagation in the second one (Figs. 6 and 7). At $h_{36}$, the tissue experienced strain ($\varepsilon_{p3}$, $\gamma_{max}$) exceeding 0.5%, with microcracks formation. After that, the microcracks propagate further, when stain measurements were beyond 1% ($\varepsilon_{p3}$, $\gamma_{max}$). This trend of increasing strain is consistent to the reports in Peña-Fernández et al. (2018b), where the tissue was exposed to Synchrotron X-ray (SR-XCT) radiation. In that case, $\varepsilon_{p1}$ reached 0.15% after the second scanned and it increased to 0.5% after the fifth one. Bone specimens of that study (Peña Fernández et al., 2018) were exposed for approximately 80 min to the radiation of the polychromatic pink beam, whereas here they were exposed (polychromatic X-ray) for 69 h.

Another parameter to be considered is the hydration status of the tissue that might also affect the strain and microcrack accumulation. In the current study the specimens were embedded in epoxy resin and kept dehydrated throughout the procedure, however, the irradiation difference cannot be assessed with certainty since the dose of radiation could not be computed in this study, as the information needed for the dose estimation could not be disclosed by the lab-XCT manufacturer. The dose of radiation in a laboratory-based XCT system depends on the energy, the pixel size, detector filter, exposure time and number of projections (Meganck and Liu, 2017). Particularly, in higher-resolution scans where bone morphological measurement are needed, an increased dose is required (Arentsen and Hui, 2013). An experiment performed on mice hind limb with an XCT tomogram *in vivo* with a duration of 19 min total scan, showed trabecular bone loss with total radiation 776 mGy (Laperre et al., 2011). In a different study it was observed that the trabecular bone volume of mice was reduced after irradiation of 712 mGy at 1, 2, 3 and 5 weeks) (Klinck et al., 2008). It has also been reported that radiation doses of 15–20 Gy at the abdomen of mice can lead to deterioration the skeleton outside the radiation field resulting in femoral and tibial bone loss, due to suppression of bone-formation activity (Jia et al., 2011). Additionally, it was found that tibial bone strength loss was twice as great as the bone loss 7 days post-irradiation.

The reduction in mechanical properties in trabecular bone specimens, due to irradiation, has been assessed in a SR-XCT system before (Peña Fernández et al., 2018). At 32.9 kGy radiation dose the apparent bone volume decreased and the strain, obtained with DVC, increased compared to the specimens irradiated at 4.7 kGy (Peña Fernández et al., 2018).

The strain distribution in the overview tomograms (DVC control, S2) did not exceed 0.2% for $\gamma_{max}$ and −0.18% for $\varepsilon_{p3}$, values that are associated to physiological loads in trabecular bone (Hunt and Donnelly, 2016; Palanca et al., 2017). Thus, it was observed that 9 h of exposure to radiation did not lead to crack initiation and degradation of the mechanical properties. Additionally, the fact that there were no cracks present in the control specimen indicates that the indentation did not cause the crack formation.

The initiation of microcracks from the edges of the trabeculae could be either a result of the effect of the X-ray radiation on the mechanical properties of the bone, or the epoxy surrounding the tissue. In this sense, the radiation-thermal effects on mechanical properties of epoxy film polymer have been previously investigated (Nguyen et al., 2017) for specimens exposed to different rates of X-ray radiation, ranging from 0 to 300 kGy. The Young's modulus of the epoxy at zero exposure was 4.84 MPa, it reached 5.86 MPa at 100 kGy and 5.34 MPa at 300 kGy. At higher irradiation dose, the mechanical properties decreased due to the polymer chain scission reactions. In the case of the current study, the elastic modulus of the epoxy resin surrounding the bone was measured throughout the process and showed no significant difference during all the stages of the protocol, with a median of 3.8 ± 0.038 GPa. It can be therefore assumed that the movement of the polymer chains remained relatively the same, since it has been shown that an increase in the movement accounts for decrease in the modulus. In this study the cracks

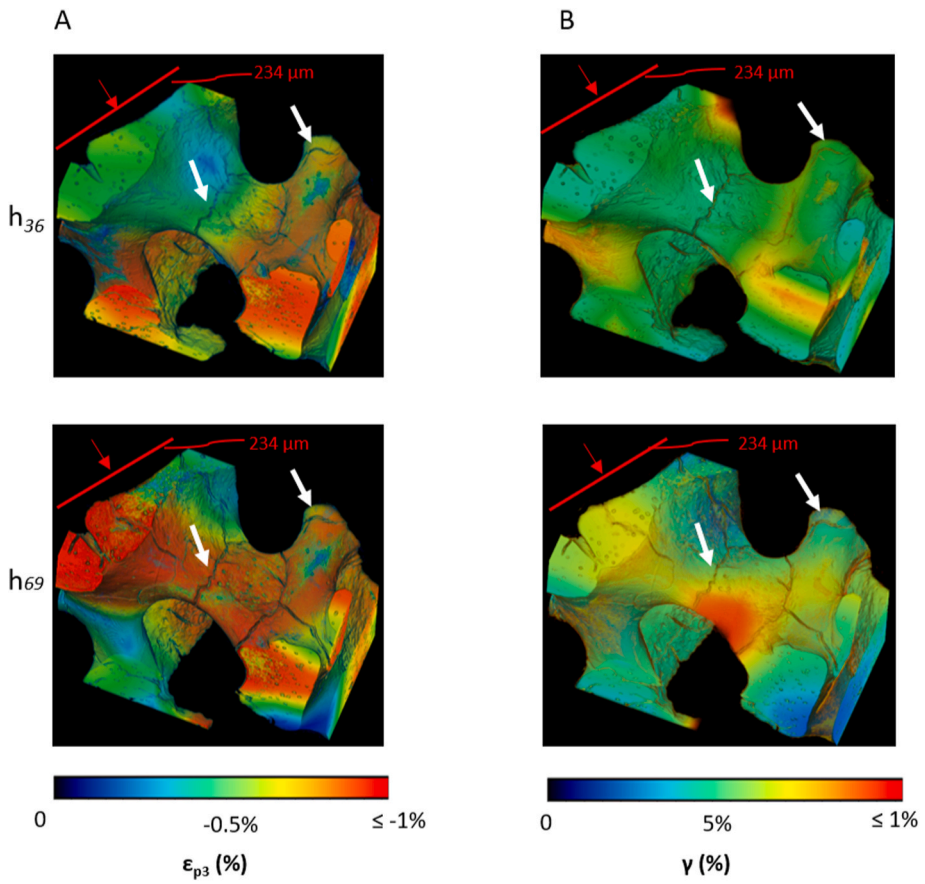


**Fig. 7.** DVC analysis of S5, where red line identifies the indentation plane and red arrow direction (234 μm apart from represented the volume). A) 3rd principal strain ($\varepsilon_{p3}$) at 36 and 69 h of exposure to radiation reaching ~ -0.8% at areas of crack formation (white arrows) and exceeding −1% at crack propagation, respectively. B) maximum shear strain ($\gamma_{max}$) at the same time points, reaching ~0.55% around the cracks (white arrows) at 36 h and approaching ~0.9% after 69 h.

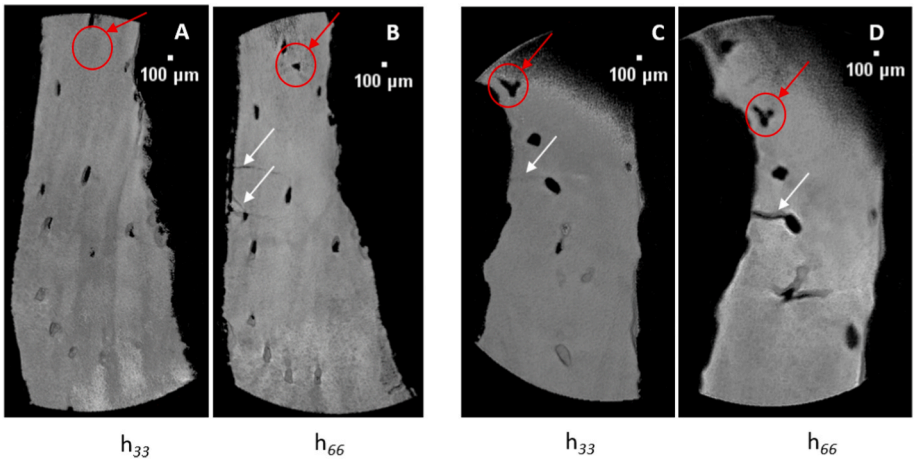


**Fig. 8.** High-resolution Zoom in Scans (0.18 μm pixel size) of S3 (A, B) and S4 (C, D) at $h_{33}$ and $h_{66}$; (A, B): the indent was applied in the 3rd indentation set and crack formation appeared after $h_{33}$. (C, D): the indent was applied in the 1st indentation set and crack formation started at $h_{33}$, propagating further at $h_{66}$; red arrows pointing at indentation imprint on the surface of the bone, white arrows showing cracks due to irradiation.

seen in the zoom-in scans of S3 and S4 are be attributed to the radiation and not the potential contraction or expansion of the epoxy resin (Fig. 8).

Bone due to its microstructure, is known to fracture under tensile, shear and compressive strains (Currey, 2002). The tensile strains could not be computed here, nevertheless, this comparative study investigated the compressive and shearing behaviour of trabecular bone as means of identifying the effect of irradiation compared to non-irradiated specimens and showed the important effect that irradiation has on bones' material properties. In the future the tensile strain could also be measured as bone is prone to fracture in Mode 1.

This study has a number of limitations. The number of indents obtained after the specimen diameter was reduced to 1 mm was limited due to the tissue surface available, and did not allow for a statistical analysis. Therefore, in order to generalise the findings, the protocol should be implemented on a larger number of specimens in the future.

Furthermore, the signal-to-noise ratio (SNR) in the high-resolution zoom in scans was not adequate to achieve an accurate DVC analysis of the specimens. High-resolution scans using SR-XCT provide a better SNR, making it easier to track changes in the volume but at a higher flux and increased tissue damage (Peña Fernández et al., 2018).

## 5. Conclusions

In conclusion, this study presents an experimental approach to evaluate the degradation in the trabecular bone mechanical properties due to X-ray irradiation combining indentation and XCT imaging. The DVC analysis in all the specimens shows higher strain accumulation as the exposure time is increased, with peak values corresponding to the formation cracks. The findings of this study can be used to inform experimental protocols in the future, to avoid damage of the tissue due to irradiation in long XCT-based experiments.

## CRediT authorship contribution statement

**Aikaterina Karali:** Writing – review & editing, Writing – original draft, Visualization, Validation, Project administration, Methodology, Investigation, Formal analysis, Data curation, Conceptualization. **Enrico Dall'Ara:** Writing – review & editing, Supervision, Resources, Methodology, Funding acquisition, Conceptualization. **Jurgita Zekonyte:** Writing – review & editing, Writing – original draft, Supervision, Resources, Project administration, Methodology, Investigation, Formal analysis, Data curation, Conceptualization. **Alexander P. Kao:** Investigation, Data curation. **Gordon Blunn:** Writing – review & editing, Validation, Supervision, Resources, Project administration, Investigation, Funding acquisition. **Gianluca Tozzi:** Writing – original draft, Supervision, Funding acquisition, Conceptualization.

## Declaration of competing interest

The authors declare that they have no known competing financial interests or personal relationships that could have appeared to influence the work reported in this paper.

## Data availability

Data will be made available on request.

## Acknowledgments

The authors would like to acknowledge Mr Geoff Britton for his assistance with the specimen preparation and experimental set up, Dr Dave Hollis (LaVision Ltd) for advice on DVC computation and Ms Yordana Shopova for proofreading the manuscript. The Insigneo Institute (University of Sheffield) provided the equipment for the specimen preparation. The Zeiss Global Centre (University of Portsmouth) provided XCT imaging and DVC capability to conduct this study. Nanoindentation equipment provided by School of Mechanical and Design Engineering (University of Portsmouth). This study is part of a PhD programme funded by the Faculty of Technology (University of Portsmouth). The authors also acknowledge the Engineering and Physical Sciences Research Council (EPSRC) funded Frontier Multisim Grant (EP/K03877X/1 and EP/S032940/1) for partial funding.

## Appendix A. Supplementary data

Supplementary data to this article can be found online at https://doi.org/10.1016/j.jmbbm.2022.105636.

## References

Akkus, O., Belaney, R.M., Das, P., 2005. Free radical scavenging alleviates the biomechanical impairment of gamma radiation sterilized bone tissue. J. Orthop. Res. 23, 838–845. https://doi.org/10.1016/j.orthres.2005.01.007.

Arentsen, L., Hui, S., 2013. Characterization of rotating gantry micro-CT configuration for the in vivo evaluation of murine trabecular bone. Microsc. Microanal. 19, 907–913. https://doi.org/10.1017/S1431927613001396.

Barth, H.D., Launey, M.E., MacDowell, A.A., Ager, J.W., Ritchie, R.O., 2010. On the effect of X-ray irradiation on the deformation and fracture behavior of human cortical bone. Bone 46, 1475–1485. https://doi.org/10.1016/j.bone.2010.02.025.

Barth, H.D., Zimmermann, E.A., Schaible, E., Tang, S.Y., Alliston, T., Ritchie, R.O., 2011. Characterization of the effects of x-ray irradiation on the hierarchical structure and mechanical properties of human cortical bone. Biomaterials 32, 8892–8904. https://doi.org/10.1016/j.biomaterials.2011.08.013.

Bay, B.K., Smith, T.S., Fyhrie, D.P., Saad, M., 1999. Digital volume correlation: three-dimensional strain mapping using x-ray tomography. Exp. Mech. 39, 217–226. https://doi.org/10.1007/BF02323555.

Boivin, G., Bala, Y., Doublier, A., Farlay, D., Ste-Marie, L.G., Meunier, P.J., Delmas, P.D., 2008. The role of mineralization and organic matrix in the microhardness of bone tissue from controls and osteoporotic patients. Bone 43, 532–538. https://doi.org/10.1016/j.bone.2008.05.024.

Bonithon, R., Kao, A.P., Fernández, M.P., Dunlop, J.N., Blunn, G.W., Witte, F., Tozzi, G., 2021. Multi-scale mechanical and morphological characterisation of sintered porous magnesium-based scaffolds for bone regeneration in critical-sized defects. Acta Biomater. 127, 338–352. https://doi.org/10.1016/j.actbio.2021.03.068.

Buckwalter, J.A., Glimcher, M.J., Cooper, R.R., Recker, R., 1995. Bone Biology 1256–1275.

Chappard, C., Basillais, A., Benhamou, L., Bonassie, A., Brunet-Imbault, B., Bonnet, N., Peyrin, F., 2006. Comparison of synchrotron radiation and conventional x-ray microcomputed tomography for assessing trabecular bone microarchitecture of human femoral heads. Med. Phys. 33, 3568–3577. https://doi.org/10.1118/1.2256069.

Currey, J.D., 2002. Bones, second ed. Princeton University Press, New Jersey.

Dall'Ara, E., Karl, C., Mazza, G., Franzoso, G., Vena, P., Pretterklieber, M., Pahr, D., Zysset, P., 2013. Tissue properties of the human vertebral body sub-structures evaluated by means of microindentation. J. Mech. Behav. Biomed. Mater. 25, 23–32. https://doi.org/10.1016/j.jmbbm.2013.04.020.

Dall'Ara, E., Öhman, C., Baleani, M., Viceconti, M., 2007. The effect of tissue condition and applied load on Vickers hardness of human trabecular bone. J. Biomech. 40, 3267–3270. https://doi.org/10.1016/j.jbiomech.2007.04.007.

Dall'Ara, E., Schmidt, R., Zysset, P., 2012. Microindentation can discriminate between damaged and intact human bone tissue. Bone 50, 925–929. https://doi.org/10.1016/j.bone.2012.01.002.

Franzoso, G., Zysset, P.K., 2008. Elastic anisotropy of human cortical bone secondary osteons measured by nanoindentation. J. Biomech. Eng. 131, 021001 https://doi.org/10.1115/1.3005162.

Gillard, F., Boardman, R., Mavrogordato, M., Hollis, D., Sinclair, I., Pierron, F., Browne, M., 2014. The application of digital volume correlation (DVC) to study the microstructural behaviour of trabecular bone during compression. J. Mech. Behav. Biomed. Mater. 29, 480–499. https://doi.org/10.1016/j.jmbbm.2013.09.014.

Harrison, N.M., McDonnell, P.F., O'Mahoney, D.C., Kennedy, O.D., O'Brien, F.J., McHugh, P.E., 2008. Heterogeneous linear elastic trabecular bone modelling using micro-CT attenuation data and experimentally measured heterogeneous tissue properties. J. Biomech. 41, 2589–2596. https://doi.org/10.1016/j.jbiomech.2008.05.014.

Hengsberger, S., Enstroem, J., Peyrin, F., Zysset, P., 2003. How is the indentation modulus of bone tissue related to its macroscopic elastic response? A validation study. J. Biomech. 36, 1503–1509. https://doi.org/10.1016/S0021-9290(03)00131-3.

Hoffler, C.E., Moore, K.E., Kozloff, K., Zysset, P.K., Brown, M.B., Goldstein, S.A., 2000. Heterogeneity of bone lamellar-level elastic moduli. Bone 26, 603–609.

Huja, S.S., Beck, F.M., Thurman, D.T., 2006. Indentation properties of young and old osteons. Calcif. Tissue Int. 78, 392–397. https://doi.org/10.1007/s00223-006-0025-3.

Hunt, H.B., Donnelly, E., 2016. Bone quality assessment techniques: geometric, compositional, and mechanical characterization from macroscale to nanoscale. Clin. Rev. Bone Miner. Metabol. 14, 133–149. https://doi.org/10.1007/s12018-016-9222-4.

Ibrahim, A., Magliulo, N., Groben, J., Padilla, A., Akbik, F., Abdel Hamid, Z., 2020. Hardness, an important indicator of bone quality, and the role of collagen in bone hardness. J. Funct. Biomater. 11, 85. https://doi.org/10.3390/jfb11040085.

Jae-young, R., Kuhn-Spearing, L., Zioupos, P., 1998. Mechanical Properties and the hierarchical structure of bone. Med. Eng. Phys. 20, 92–102. https://doi.org/10.1038/251673a0.

Jia, D., Gaddy, D., Suva, L.J., Corry, P.M., 2011. Rapid loss of bone mass and strength in mice after abdominal irradiation. Radiat. Res. 176, 624–635. https://doi.org/10.1667/rr2505.1.

Judex, S., Boyd, S., Qin, Y.X., Miller, L., Müller, R., Rubin, C., 2003. Combining high-resolution micro-computed tomography with material composition to define the quality of bone tissue. Curr. Osteoporos. Rep. 1, 11–19. https://doi.org/10.1007/s11914-003-0003-x.

Karali, A., Kao, A.P., Meeson, R., Roldo, M., Blunn, G.W., Tozzi, G., 2020. Full-field strain of regenerated bone tissue in a femoral fracture model. J. Microsc. 1–11. https://doi.org/10.1111/jmi.12937.

Karali, A., Kao, A.P., Zekonyte, J., Blunn, G., Tozzi, G., 2021. Micromechanical evaluation of cortical bone using in situ XCT indentation and digital volume correlation. J. Mech. Behav. Biomed. Mater. 115, 104298 https://doi.org/10.1016/j.jmbbm.2020.104298.

Klinck, R.J., Campbell, G.M., Boyd, S.K., 2008. Radiation effects on bone architecture in mice and rats resulting from in vivo micro-computed tomography scanning. Med. Eng. Phys. 30, 888–895. https://doi.org/10.1016/j.medengphy.2007.11.004.

Laperre, K., Depypere, M., van Gastel, N., Torrekens, S., Moermans, K., Bogaerts, R., Maes, F., Carmeliet, G., 2011. Development of micro-CT protocols for in vivo follow-up of mouse bone architecture without major radiation side effects. Bone 49, 613–622. https://doi.org/10.1016/j.bone.2011.06.031.

Levrero-Florencio, F., Margetts, L., Sales, E., Xie, S., Manda, K., Pankaj, P., 2016. Evaluating the macroscopic yield behaviour of trabecular bone using a nonlinear homogenisation approach. J. Mech. Behav. Biomed. Mater. 61, 384–396. https://doi.org/10.1016/j.jmbbm.2016.04.008.

Lowe, T., Avcu, E., Bousser, E., Sellers, W., Withers, P.J., 2018. 3D Imaging of indentation damage in bone. Materials 11, 1–13. https://doi.org/10.3390/ma11122533.

Lucchini, R., Carnelli, D., Ponzoni, M., Bertarelli, E., Gastaldi, D., Vena, P., 2011. Role of damage mechanics in nanoindentation of lamellar bone at multiple sizes: experiments and numerical modeling. J. Mech. Behav. Biomed. Mater. 4, 1852–1863. https://doi.org/10.1016/j.jmbbm.2011.06.002.

Martínez-Reina, J., Domínguez, J., García-Aznar, J.M., 2011. Effect of porosity and mineral content on the elastic constants of cortical bone: a multiscale approach. Biomech. Model. Mechanobiol. 10, 309–322. https://doi.org/10.1007/s10237-010-0236-4.

Meganck, J.A., Liu, B., 2017. Dosimetry in micro-computed tomography: a review of the measurement methods, impacts, and characterization of the quantum GX imaging system. Mol. Imag. Biol. 19, 499–511. https://doi.org/10.1007/s11307-016-1026-x.

Mirzaali, M.J., Schwiedrzik, J.J., Thaiwichai, S., Best, J.P., Michler, J., Zysset, P.K., Wolfram, U., 2016. Mechanical properties of cortical bone and their relationships with age, gender, composition and microindentation properties in the elderly. Bone 93, 196–211. https://doi.org/10.1016/j.bone.2015.11.018.

Nguyen, A.T., Visakh, P.M., Nazarenko, O.B., Chandran, C.S., Melnikoca, T.V., 2017. Effect of electron beam irradiation on thermal and mechanical properties of epoxy polymer. Conf. Ser. Mater. Sci. Eng. 168, 1–7. https://doi.org/10.1088/1757-899X/168/1/012073.

Nguyen, H., Morgan, D.A.F., Forwood, M.R., 2007. Sterilization of allograft bone: effects of gamma irradiation on allograft biology and biomechanics. Cell Tissue Bank. 8, 93–105. https://doi.org/10.1007/s10561-006-9020-1.

Oftadeh, R., Perez-Viloria, M., Villa-Camacho, J.C., Vaziri, A., Nazarian, A., 2015. Biomechanics and mechanobiology of trabecular bone: a review. J. Biomech. Eng. 137, 010802 https://doi.org/10.1115/1.4029176.

Oliver, W.C., Pharr, G.M., 2004. Measurement of hardness and elastic modulus by instrumented indentation: advances in understanding and refinements to methodology. J. Mater. Res. 19, 3–20. https://doi.org/10.1557/jmr.2004.19.1.3.

Palanca, M., Bodey, A.J., Giorgi, M., Viceconti, M., Lacroix, D., Cristofolini, L., Dall'Ara, E., 2017. Local displacement and strain uncertainties in different bone types by digital volume correlation of synchrotron microtomograms. J. Biomech. 58, 27–36. https://doi.org/10.1016/j.jbiomech.2017.04.007.

Palanca, M., Tozzi, G., Cristofolini, L., 2016. The use of digital image correlation in the biomechanical area: a review. Int. Biomech. 3, 1–21. https://doi.org/10.1080/23335432.2015.1117395.

Palanca, M., Tozzi, G., Cristofolini, L., Viceconti, M., Dall'Ara, E., 2015. Three-dimensional local measurements of bone strain and displacement: comparison of three digital volume correlation approaches. J. Biomech. Eng. 137, 071006 https://doi.org/10.1115/1.4030174.

Peña-Fernández, M., Barber, A.H., Blunn, G.W., Tozzi, G., 2018a. Optimization of digital volume correlation computation in SR-microCT images of trabecular bone and bone-biomaterial systems. J. Microsc. 272, 213–228. https://doi.org/10.1111/jmi.12745.

Peña-Fernández, M., Dall'Ara, E., Kao, A.P., Bodey, A.J., Karali, A., Blunn, G.W., Barber, A.H., Tozzi, G., Peña Fernández, M., Ara, E.D., Kao, A.P., Bodey, A.J., Karali, A., Blunn, G.W., Barber, A.H., Tozzi, G., 2018b. Preservation of bone tissue integrity with temperature control for in situ SR-MicroCT experiments. Materials 11. https://doi.org/10.3390/ma11112155.

Peña Fernández, M., Cipiccia, S., Dall'Ara, E., Bodey, A.J., Parwani, R., Pani, M., Blunn, G.W., Barber, A.H., Tozzi, G., 2018. Effect of SR-microCT radiation on the mechanical integrity of trabecular bone using in situ mechanical testing and digital volume correlation. J. Mech. Behav. Biomed. Mater. 88, 109–119. https://doi.org/10.1016/j.jmbbm.2018.08.012.

Peña Fernández, M., Dall'Ara, E., Bodey, A.J., Parwani, R., Barber, A.H., Blunn, G.W., Tozzi, G., 2019. Full-field strain analysis of bone-biomaterial systems produced by the implantation of osteoregenerative biomaterials in an ovine model. ACS Biomater. Sci. Eng. 5, 2543–2554. https://doi.org/10.1021/acsbiomaterials.8b01044.

Rho, J.Y., Roy, M.E., Tsui, T.Y., Pharr, G.M., 1999. Elastic properties of microstructural components of human bone tissue as measured by nanoindentation. J. Biomed. Mater. Res. 45, 48–54. https://doi.org/10.1002/(SICI)1097-4636(199904)45:1<48::AID-JBM7>3.0.CO;2-5.

Rodriguez-Florez, N., Oyen, M.L., Shefelbine, S.J., 2013. Insight into differences in nanoindentation properties of bone. J. Mech. Behav. Biomed. Mater. 18, 90–99. https://doi.org/10.1016/j.jmbbm.2012.11.005.

Roy, M.E., Rho, J.Y., Tsui, T.Y., Evans, N.D., Pharr, G.M., 1999. Mechanical and morphological variation of the human lumbar vertebral cortical and trabecular bone. J. Biomed. Mater. Res. 44, 191–197. https://doi.org/10.1002/(SICI)1097-4636(199902)44:2<191::AID-JBM9>3.0.CO;2-G.

Samuel, J., Sinha, D., Zhao, J.C.G., Wang, X., 2014. Water residing in small ultrastructural spaces plays a critical role in the mechanical behavior of bone. Bone 59, 199–206. https://doi.org/10.1016/j.bone.2013.11.018.

Swadener, J.G., Rho, J.Y., Pharr, G.M., 2001. Effect of anisotropy on elastic moduli measured by nanoindentation in human tibial cortical bone. J. Biomed. Mater. Res. 57, 108–112. https://doi.org/10.1002/1097-4636(200110)57:1<108::AID-JBM1148>3.0.CO;2-6.

Tozzi, G., Dall'Ara, E., Palanca, M., Curto, M., Innocente, F., Cristofolini, L., 2017. Strain uncertainties from two digital volume correlation approaches in prophylactically augmented vertebrae: local analysis on bone and cement-bone microstructures. J. Mech. Behav. Biomed. Mater. 67, 117–126. https://doi.org/10.1016/j.jmbbm.2016.12.006.

Tozzi, G., Danesi, V., Palanca, M., Cristofolini, L., 2016. Elastic full-field strain analysis and microdamage progression in the vertebral body from digital volume correlation. Strain 52, 446–455. https://doi.org/10.1111/str.12202.

Tozzi, G., Peña Fernández, M., Davis, S., Karali, A., Kao, A.P., Blunn, G.W., 2020. Full-field strain uncertainties and residuals at the cartilage-bone interface in unstained tissues using propagation-based phase-contrast XCT and digital volume correlation. Materials. https://doi.org/10.3390/ma13112579. Under Revi, 1–15.

Tozzi, G., Zhang, Q.H., Tong, J., 2014. Microdamage assessment of bone-cement interfaces under monotonic and cyclic compression. J. Biomech. 47, 3466–3474. https://doi.org/10.1016/j.jbiomech.2014.09.012.

Viguet-Carrin, S., Garnero, P., Delmas, P.D., 2006. The role of collagen in bone strength. Osteoporos. Int. 17, 319–336. https://doi.org/10.1007/s00198-005-2035-9.

Wang, X., Bank, R.A., TeKoppele, J.M., Mauli Agrawal, C., 2001. The role of collagen in determining bone mechanical properties. J. Orthop. Res. 19, 1021–1026. https://doi.org/10.1016/S0736-0266(01)00047-X.

Wolfram, U., Wilke, H.-J., Zysset, P.K., 2010a. Transverse isotropic elastic properties of vertebral trabecular bone matrix measured using microindentation under dry conditions (effects of age, gender, and vertebral level). J. Mech. Med. Biol. 10, 139–150. https://doi.org/10.1142/s0219519410003241.

Wolfram, U., Wilke, H.J., Zysset, P.K., 2010b. Valid μ finite element models of vertebral trabecular bone can be obtained using tissue properties measured with nanoindentation under wet conditions. J. Biomech. https://doi.org/10.1016/j.jbiomech.2010.02.026.

Wolfram, U., Wilke, H.J., Zysset, P.K., 2010c. Rehydration of vertebral trabecular bone: influences on its anisotropy, its stiffness and the indentation work with a view to age, gender and vertebral level. Bone 46, 348–354. https://doi.org/10.1016/j.bone.2009.09.035.

Zhang, J., Michalenko, M.M., Kuhl, E., Ovaert, T.C., 2010. Characterization of indentation response and stiffness reduction of bone using a continuum damage model. J. Mech. Behav. Biomed. Mater. 3, 189–202. https://doi.org/10.1016/j.jmbbm.2009.08.001.

Zysset, P.K., 2009. Indentation of bone tissue: a short review. Osteoporos. Int. 20, 1049–1055. https://doi.org/10.1007/s00198-009-0854-9.

Zysset, P.K., 2003. A review of morphology-elasticity relationships in human trabecular bone: theories and experiments. J. Biomech. 36, 1469–1485. https://doi.org/10.1016/S0021-9290(03)00128-3.